Molecular properties of (U)LIRGs: CO, HCN, HNC and HCO$^+$

A. F. Loenen[1,2], W. A. Baan[2] and M. Spaans[1]

[1]Kapteyn Astronomical Institute, University of Groningen,
P.O. Box 800, 9700 AV Groningen, The Netherlands
email: loenen@astro.rug.nl, spaans@astro.rug.nl

[2]ASTRON, P.O. Box 2, 7990 AA Dwingeloo, The Netherlands
email: baan@astron.nl

Abstract. The observed molecular properties of a sample of FIR-luminous and OH megamaser (OH-MM) galaxies have been investigated. The ratio of high and low-density tracer lines is found to be determined by the progression of the star formation in the system. The HCO$^+$/HCN and HCO$^+$/HNC line ratios are good proxies for the density of the gas, and PDR and XDR sources can be distinguished using the HNC/HCN line ratio. The properties of the OH-MM sources in the sample can be explained by PDR chemistry in gas with densities higher than $10^{5.5}$ cm^{-3}, confirming the classical OH-MM model of IR pumped amplification with (variable) low gains.

Keywords. galaxies: nuclei, galaxies: ISM, galaxies: active, galaxies: starburst, ISM: molecules, ISM: evolution, radio lines: ISM

1. Introduction

High-density molecular gas plays an important role in the physics of (Ultra-)Luminous Infrared Galaxies ((U)LIRGs), giving rise to spectacular starbursts and possibly providing the fuel for an active galactic nucleus (AGN). The emission lines emanating from the nuclear gas provide information about the physical properties of the nuclear environment in these systems, e.g. the (column) density, temperature and chemical composition of the gas, and the type and strength of the central energy source. It can also provide us an insight into the processes influencing the (gas in the) nuclei: the star formation rate and history, fuelling of a possible central black hole and feedback processes.

Baan *et al.* (2007) present data of the CO, HCN, HNC, HCO$^+$, CN, and CS line emissions of a representative group of 37 FIR-luminous and OH megamaser (OH-MM) galaxies and 80 additional sources taken from the literature. In this work, the molecular characteristics of this sample are explained using several models. First, the properties of the different (density) components of the nuclear gas are explained in terms of starburst evolution (see Baan *et al.* 2007). Also the chemical properties of the high-density gas are analyzed, using chemical networks (Meijerink & Spaans 2005) and radiative transfer models Meijerink *et al.* (2007). Here only the J=1-0 transitions of the molecules are considered. A more detailed analysis will be presented in Loenen, Baan & Spaans (2007).

2. Starburst evolution

The gas in galaxies is build up from multiple components, each with different densities and temperatures. From our data we can derive information about these different components. The CO(1-0) line traces the large scale low-density (critical density $n_{\rm cr}$=3×10^3 cm^{-3}) component (LD), whereas the lines of HCN, HNC, and HCO$^+$
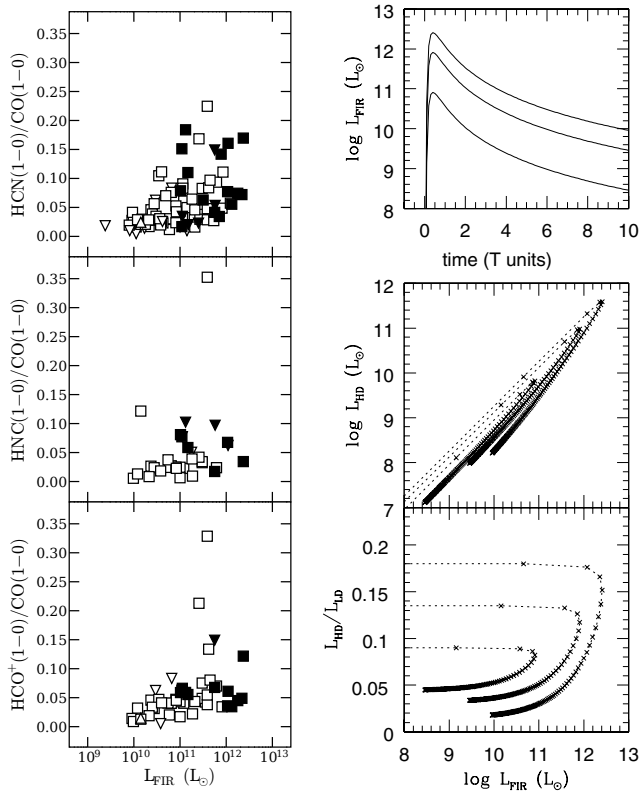
Figure 1. *left, from top to bottom:* Integrated line ratios HCN(1-0)/CO(1-0), HNC(1-0)/CO(1-0), and HCO$^+$(1-0)/CO(1-0) versus FIR luminosity. Squares represent reliable values and triangles upper or lower limits. Filled symbols are sources with OH-MM activity.
right, from top to bottom: Three FIR luminosity curves used in the simulations with different maximum luminosities, the luminosity of a high-density component, and the variation of the high- versus low-density ratio during the outburst starting at the upper part of the curve.

(all $n_{cr} > 10^5$ cm^{-3}) trace the high-density component (HD) which mostly resides in the cores of the galaxies, at the sites of the star-formation activity.

On the left hand side of Fig. 1, the relative contributions of these two density components are shown, by plotting the ratios of the high-density and CO(1-0) line strengths. The figure shows that the distribution of line ratios for all molecules increases with FIR luminosity, which gives an upwardly curved lower boundary for the distribution at higher L_{FIR}. The highest values are found at $L_{FIR} \geqslant 10^{10.5}$ L$_\odot$. The figure also shows that in general the OH-MM sources have a much larger spread in HD/CO(1-0).

This behavior can be explained as the result of ongoing star formation. The FIR luminosity of the ULIRG during the evolution of the outburst reflects energy generated by the star formation activity. The FIR luminosity integrated over the course of the outburst would reflect the amount of high-density molecular material consumed by the star formation process and destroyed or removed by feedback.

In the following simplified scenario (see Baan *et al.* 2007), we employ a model for the time-evolution of the high-density components in a galaxy during a FIR outburst. In the absence of a representative FIR light curve, we use a diffusion-like expression in time t as a response to a starburst starting at $t=0$ defined as:

$$L_{FIR}(t) = 1.35 L_{FIR}(0) \left(\frac{t}{T}\right)^{2.5} e^{-t/T}, \qquad (2.1)$$

where $L_{FIR}(0)$ is the maximum luminosity of the burst and T is the timescale of the outburst. We note that a diffusion curve may not be the most appropriate representation

of L_{FIR}, but this curve does resemble the outcome of starburst-driven FIR evolution simulations (Loenen, Baan & Spaans 2006).

The high-density component HD can be defined as β LD, the low-density component. As a result, the high-low-density ratio varies with time during the FIR outburst as:

$$\frac{\mathrm{HD}(t)}{\mathrm{LD}} = \beta \left[1 - \gamma \frac{\int L_{\mathrm{FIR}}(t)\mathrm{d}t}{L_{\mathrm{FIR,int}}} \right], \qquad (2.2)$$

where γ is the fraction of the initial HD component that is consumed during the whole outburst, and $L_{\mathrm{FIR,int}}$ the FIR luminosity integrated over the whole course of the outburst. The large-scale low-density component LD is assumed to remain unchanged.

The results of these simulations have been presented on the right hand side in Fig. 1. The top panel shows the FIR light curve of the outburst for three peak luminosities. The middle panel shows the luminosity of a representative high-density component for the three L_{FIR} curves. The bottom panel shows the high-low-density ratio for these same FIR light curves. Combining the results of this simulation with the data shows that the HD/CO(1-0) data points in the left panels are a measure of the evolution of the starburst. This implies that the OH MM sources are galaxies in an early stage of star formation, which is consistent with OH MM sources being found in starburst-dominated galaxies (Genzel *et al.* 1998; Baan & Klöckner 2007).

3. Chemistry

The model presented in the previous section does well in explaining the evolution of the different gas components, but it makes no distinction between the different high-density tracers. Even though the emission of the different molecules originates in the same regions, the line strengths are influenced by the environmental properties like the (column) density, temperature, and the type and strength of the prevailing radiation field. In order to study the effects of these parameters on the emission characteristics of the sources, we remove the intrinsic difference in line strength between the galaxies in our sample and use line ratios to find diagnostic properties. Fig. 2 presents the ratios of the integrated lines of HCO^{+}/HCN, HNC/HCO^{+} and HNC/HCN against each other.

In order to interpret the behavior of the sources in this diagram, we compare the data to the theoretical models that treat the chemistry and radiative transfer of molecular clouds, including all the relevant heating, cooling and chemical processes (see Meijerink & Spaans 2005; Meijerink *et al.* 2007, and Spaans *et al.*in these proceedings). A large grid of models was created by Meijerink *et al.* (2007), varying the strength of the radiation field, its type (UV and X-ray), the gas density and the column density. These results are compared to our observational data in Fig. 2 (note: not all models are shown, some fall out of the range of our figure).

3.1. *PDR models*

The results of the PDR models (UV radiation field) are shown in Fig. 2 with heavy lines, where the line styles indicate different gas densities (solid: $n=10^{4.5}$, dashed: $n=10^{5.0}$, and striped: $n=10^{5.5}$ cm^{-3}). The tracks vary as a function of column density, which ranges from $N=10^{22}$ cm^{-2} (the column density below which the strength of the emission lines decreases rapidly) to $N=10^{23}$, $N=10^{23.5}$ and $N=10^{24}$ cm^{-2} for the $n=10^{4.5}$, $n=10^{5.0}$, and $n=10^{5.5}$ cm^{-3} models, respectively (corresponding to a cloud size of 1 pc; indicated by the symbol at one end of the tracks). Two different radiation field strengths are shown: $F_{\mathrm{UV}}=1.6$ erg cm^{-2} s^{-1}, indicated by a plus symbol at the highest column density point, and $F_{\mathrm{UV}}=160$ erg cm^{-2} s^{-1}, indicated with a circle.
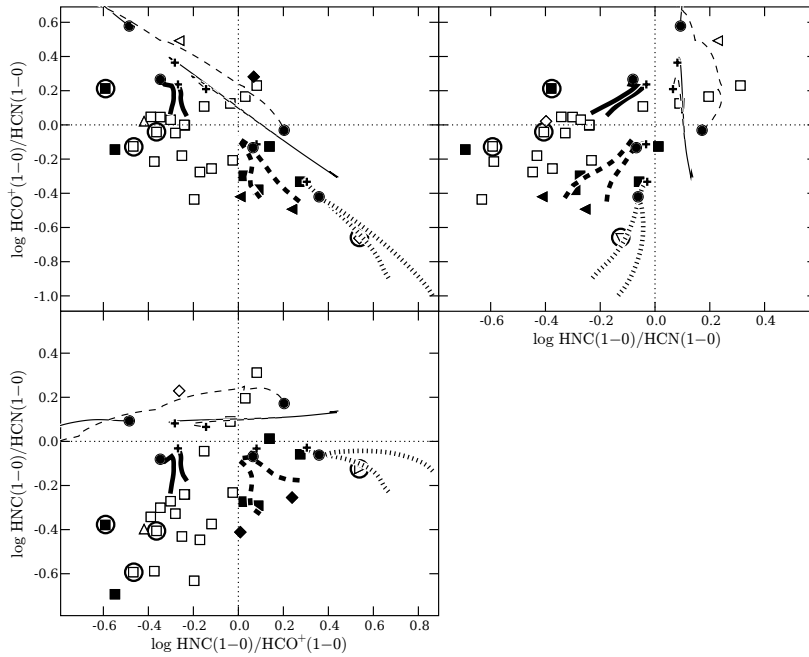
Figure 2. *top left* Integrated HCO$^+$(1-0)/HCN(1-0) versus HNC(1-0)/HCO$^+$(1-0) ratios. *top right* Integrated HCO$^+$(1-0)/HCN(1-0) versus HNC(1-0)/HCN(1-0) ratios. *bottom left* Integrated HNC(1-0)/HCN(1-0) versus HNC(1-0)/HCO$^+$(1-0) ratios. Explanation about the plot symbols and line styles is provided in Sect. 3.

Two observations can be made, when comparing the data and the models. First of all one can see that the models are separated based on the density (n) in the HCO$^+$/HCN and HCO$^+$/HNC line ratios. The HNC/HCN line ratio shows no differentiation. This can be explained in terms of the critical density of the individual molecules. HCO$^+$ has a critical density of about 3×10^5 cm^{-3}, whereas the critical density of HCN and HNC is around 3×10^6 cm^{-3}. Therefore the excitation of HCO$^+$ will differ from HCN and HNC for different densities. A second observation that can be made is that most of the OH MM sources cluster together in an area traced by PDR models that have a high-density ($n\geqslant10^{5.5}$ cm^{-3}), and a high column density $N\geqslant10^{22}$ cm^{-2}. This points to the classical OH MM model of IR (UV radiation reprocessed by the surrounding gas and dust) pumped, low (and variable) gain amplification (Baan 1989).

3.2. XDR models

The results of two XDR simulations are also shown in Fig. 2, using thin lines. Again, the line styles indicate different gas densities (solid: $n=10^{5.5}$, and dashed: $n=10^{6.0}$ cm^{-3}); column densities range from $N=10^{22}$ to $N=10^{24}$-$10^{24.5}$; and the radiation field strengths are $F_X=1.6$ (plus), and $F_X=160$ erg cm^{-2} s^{-1} (circle).

The XDR models are not as well differentiated as the PDR models. Because X-ray photons penetrate the molecular cloud much easier, the XDRs do not show the strong density dependency seen for the PDRs, making the distinction between different XDR models very difficult. The addition of higher transitions and other molecules (e.g. CN, CO$^+$, HOC$^+$) will most likely break this degeneracy. Another problem with trying to identify XDR sources is that they are in general smaller that PDR sources and thus are more affected by beam dilution, especially in single dish observations like ours. This will

affect the detection rate of XDR sources and could make hybrid sources look like PDR sources, even if the XDRs are energetically more important than the PDRs.

Despite these drawbacks, the XDR models do provide diagnostics, since they clearly separate from the PDR models in their HNC/HCN line ratio. The PDR models approach, but never cross the HNC/HCN=1 line and the XDR models all have HNC/HCN>1. Therefore, the HNC/HCN line ratio is an excellent way to determine whether a system's chemistry is dominated by UV or X-ray photons.

3.3. *Terra Incognita*

Not all our observational data in Fig. 2 is covered by the models. The few sources in our sample with known H_2O MM activity (indicated by plot symbols surrounded by circles) are also located in this area, which is characterized by lower HNC and higher HCO^+ line strengths compared to HCN. The fact that this area is not covered by the models suggests that other processes influence the line ratios, such as strong shocks. Shocks are not treated in the models and can have profound effects on the chemistry in molecular clouds as they may selectively destroy HNC (Schilke *et al.* 1992) and enhance HCO^+ relative to HCN (Dickinson *et al.* 1980). A simultaneous increase in HCO^+ and a decrease in HNC shifts the PDR models to the uncovered region, implying that the H_2O MM sources in our sample are UV driven systems with strong shocks. This would suggest that these H_2O MM sources are similar to shock-induced Galactic H_2O maser spots (see other contributions in these proceedings).

4. Conclusions

Molecular line emissions of multiple species (and transitions) provide excellent diagnostics for understanding the status of the nuclear gas in extra-galactic sources. The different molecules trace different (density) components and the ratio of high and low-density tracer lines follows the star formation activity in the system. Comparing different high-density tracers tells a lot about physical characteristics of the gas. The HCO^+/HCN and HCO^+/HNC line ratios are good proxies for the density of the gas, due to the different critical densities of the species. PDR and XDR sources can be distinguished using the HNC/HCN line ratio: PDR sources all have ratios lower than unity and XDRs have ratios larger than 1. OH MM sources cluster in a particular part of the diagnostic diagram, which is only traced by PDR models with densities higher than $10^{5.5}\,\mathrm{cm}^{-3}$, confirming the classical OH MM model of FIR (UV radiation reprocessed by the surrounding gas and dust) pumped amplification with low but variable gains.

References

Baan, W. A. 1989, *ApJ* 338, 804
Baan, W. A., Henkel, C., Loenen, A. F., Baudry, A., & Wiklind, T. 2007, submitted to *A&A*
Baan, W. A., & Klöckner, H.-R. 2006, *A&A*, 449, 559
Dickinson, D. F., Dinger, A. S. C., Kuiper, T. B. H., & Rodriguez Kuiper, E. N. 1980, *ApJ*, 237, L43
Genzel, R., *et al.* 1998, *ApJ* 4498, 579
Loenen, A. F., Baan, W., A., & Spaans, M. 2006, *A&A* 458, 89
Loenen, A. F., Baan, W., A., & Spaans, M. 2007, in preparation
Meijerink, R., & Spaans, M. 2005, *A&A* 436, 397
Meijerink, R., Spaans, M., & Israel, F. P. 2007, *A&A* 461, 793
Schilke, P., Walmsley, C. M., Pineau Des Forets, G. *et al.* 1992, *A&A* 256, 595